Journal of Coastal Research	00	0	000–000	Coconut Creek, Florida	Month 0000

Salt-Wedge Response to Variable River Flow and Sea-Level Rise in the Microtidal Rječina River Estuary, Croatia

Nino Krvavica*, Vanja Travaš, and Nevenka Ožanić

Faculty of Civil Engineering
University of Rijeka
Rijeka 51000, Croatia

www.cerf-jcr.org

www.JCRonline.org

ABSTRACT

Krvavica, N.; Travaš, V., and Ožanić, N., 0000. Salt-wedge response to variable river flow and sea-level rise in the microtidal Rječina River Estuary, Croatia. *Journal of Coastal Research,* 00(0), 000–000. Coconut Creek (Florida), ISSN 0749-0208.

A finite-volume model for two-layer shallow-water flow is presented and applied to study the dynamic response of a salt wedge in a microtidal estuary to changes in river flow rate and sea-level rise (SLR). First, the shape of the arrested salt wedge was computed for different hydrographic conditions. Next, the response of the salt wedge to highly variable river flow was investigated. Finally, this model was applied to predict the impacts of the SLR on salinity intrusions in the Rječina River Estuary. To assess the model performance and to examine the salinity structure in the estuary, a field-sampling campaign was conducted during 2014 and 2015. Field observations revealed negligible longitudinal density variations in both freshwater and saltwater layers and highly stratified conditions for all considered river flow rates and sea levels. Furthermore, the maximum buoyancy frequency, computed as a measure of vertical stratification, was among the highest ever reported in field investigations. The behavior of the salt-wedge intrusion depends mainly on the river flow rate, although sea level and channel geometry become more influential under low-flow conditions. Computed salt-wedge shapes and propagation rates agreed well with field observations. The salinity structure in the Rječina River Estuary is not expected to change in the future for tested SLR scenarios, although stronger salt-wedge intrusion is predicted by the numerical model.

ADDITIONAL INDEX WORDS: *Stratification, two-layer, numerical model, shallow-water equation, finite-volume method*.

INTRODUCTION

Salt-wedge estuaries usually develop at the mouths of coastal rivers where the ratio of river to tidal flow is high enough to maintain a strong density stratification (Hansen and Rattray Jr., 1966). Under ideal conditions, an upper layer of freshwater would be separated from a lower layer of seawater by a sharp halocline, with the overriding flow pushing the underlying one toward the river mouth until an equilibrium is achieved between the buoyancy pressure gradient, friction forces, and inertial forces (Sargent and Jirka, 1987). For steady-flow conditions, *i.e.* constant sea levels and river flow rates, a so-called arrested salt wedge would eventually be established where only the upper layer is active; however, steady states rarely occur in the natural environment because of the continuous influence of tidal motions.

A pronounced vertical stratification occurs in many salt-wedge estuaries worldwide (*e.g.,* the Mississippi, Merrimack, Fraser, and Rhone Rivers) and is maintained by high river flow rates, which dampen the extent of vertical mixing caused by tidal motions (Geyer and MacCready, 2014; Ibanez, Pont, and Prat, 1997). Notably, the salt-wedge structure in the Fraser Estuary is observed only during very high river flow rates (MacDonald and Geyer, 2004); however, in microtidal seas (<2 m), which are common in the Mediterranean region, estuaries are highly stratified even for relatively low river flow rates. A typical example of such a microtidal salt-wedge estuary is the Ebro River in Spain (Ibanez, Pont, and Prat, 1997). Unfortunately, very few studies of the physical processes in such environments exist in the literature.

The Rječina River Estuary

The Rječina River is an 18.6 km long karst river located in the northern coastal part of Croatia at 45°20′ N and 14°27′ E, and it originates from a strong karst spring Rječina, situated 325 m above sea level (a.s.l.). In its lower reaches, the river flows through a narrow canyon and then continues through an alluvial plain in the city center of Rijeka, where it finally enters the Adriatic Sea (Figure 1). Water drawn from the Rječina River is mainly used for Rijeka's water supply system (WSS) and electricity production at the Hydropower Plant Rijeka (Rijeka HPP). The main intake is located at Rječina spring (at 325 m a.s.l.), from which 0.69 $m^3 s^{-1}$ is used for WSS on average every year, except in the summer months, when the spring usually dries out (Rubinić and Sarić, 2005). During these dry months, usually from June to August, the water is drawn from the second intake located at Zvir spring (at 2.85 m a.s.l.), next to the Rječina River channel, at a distance of 1.4 km from the river mouth (Figure 1). The mean annual intake from Zvir spring is 0.21 $m^3 s^{-1}$ (Rubinić and Sarić, 2005).

The water regime in the Rječina River significantly changed after the construction of the Valići dam and reservoir in the middle reaches of the river (Karleuša *et al*., 2009). Water drawn from the reservoir is used for the electricity production at the Rijeka HPP, located in the city center, near Zvir spring. The

DOI: 10.2112/JCOASTRES-D-16-00053.1 received 1 April 2016; accepted in revision 20 May 2016; corrected proofs received 22 July 2016; published pre-print online 26 August 2016.
*Corresponding author: nino.krvavica@uniri.hr

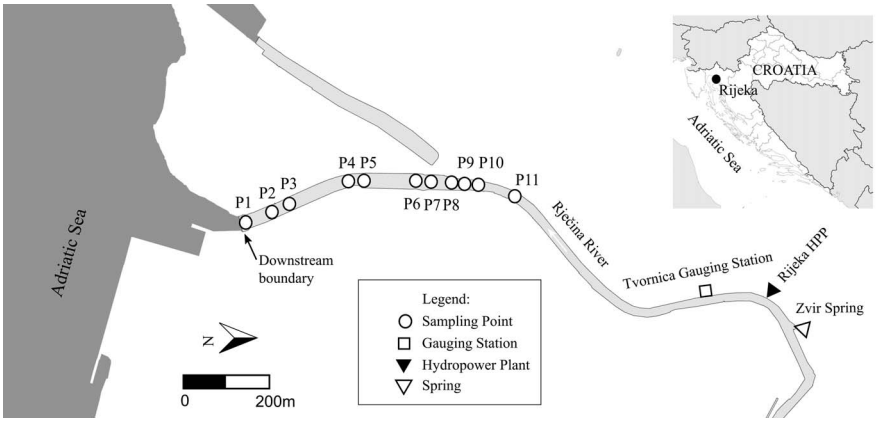

Figure 1. Map showing the Rječina River Estuary with locations of the sampling points.

maximum operating capacity of the Rijeka HPP is 21 $m^3 s^{-1}$, and the overflowed water is discharged back into the Rječina River channel at 1.3 km from the river mouth (Figure 1).

Observations during the 16-year period (1999–2015) at Tvornica gauging station, located downstream from the Rijeka HPP outflow at 1.2 km from the mouth (Figure 1), show that the mean annual flow rate (Q) in the lower reaches of the Rječina River is 11.1 $m^3 s^{-1}$. Figure 2 shows the variations in the minimum, mean, and maximum monthly flow rate throughout the year and the variation of mean annual flow. The base flow at this gauging station largely comprises overflowed waters from Rječina spring and Zvir spring, in about equal parts when the mean annual flow is considered (Rubinić and Sarić, 2005). During the summer months when Rječina Spring usually dries out, however, only Zvir spring provides the base flow, with overflows ranging from a daily minimum $Q < 0.1$ $m^3 s^{-1}$, observed in August 2003, to an average 1–2 $m^3 s^{-1}$. On the other hand, during the wet period (November to February), overflowed waters from Zvir spring amount up to 20 $m^3 s^{-1}$, contributing in part to the total water flow rate at Tvornica gauging station, where a maximum daily flow rate of 184 $m^3 s^{-1}$ was observed in February 2014. Interdaily oscillations also occur in the lower reaches because of the outflows from the Rijeka HPP, depending on their operating patterns.

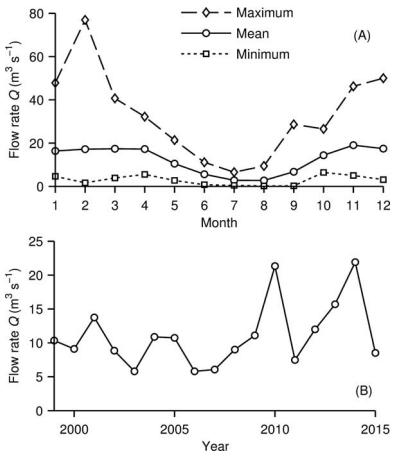

Figure 2. Interannual variation of maximum, mean, and minimum monthly flow rates (A) and variation of mean annual flow rates (B), observed at Tvornica Gaugin station (1999–2015).

The Rječina River Estuary is a typical example of a microtidal salt wedge where a variable river flow rate is the main source of its time dependence rather than tides. The estuary is characterized by a relatively short length and a steep bed slope; the maximum-recorded salt intrusion length during 2014–15 was just less than 1 km, the maximum depth near the mouth is 4.2 m, and the average bed slope is 0.4% (Figure 3). In the upper part of the estuary, the channel cross sections are narrow with vertical walls, while the cross sections are wider with mildly sloped sides and a natural bed in the middle and lower part of the estuary (Figure 4). Krvavica *et al*. (2012) showed that highly stratified conditions are observed in the Rječina River Estuary, even for low river flow rates, and that the salt wedge is expelled from the estuary when $Q > 38.1$ $m^3 s^{-1}$. Furthermore, an arrested salt wedge frequently forms in the estuary because of a specific combination of low tidal amplitudes, partially controlled freshwater flow rate, and its relatively short length.

Adriatic Sea

The Adriatic Sea is a semi-closed basin connected to the Mediterranean Sea through the Otranto Strait. The tides in the Adriatic Sea are of a mixed type with relatively low amplitudes. The maximum astronomical tidal amplitude recorded between 1953 and 2006 at the Bakar tidal gauging station, which is located only 12 km from the Rijeka city center, was 123 cm; however, mean tidal amplitudes do not exceed 30 cm (Rezo and Pavasović, 2014).

Although the effects that climate change will have in the future are unknown, all recent studies predict that global sea levels, including those of the Mediterranean and Adriatic Seas, will rise. A global sea-level rise (SLR) of 19 cm has been recorded over the period 1901–2010, with long-term projections suggesting that this increase will lie within the range of 26–82

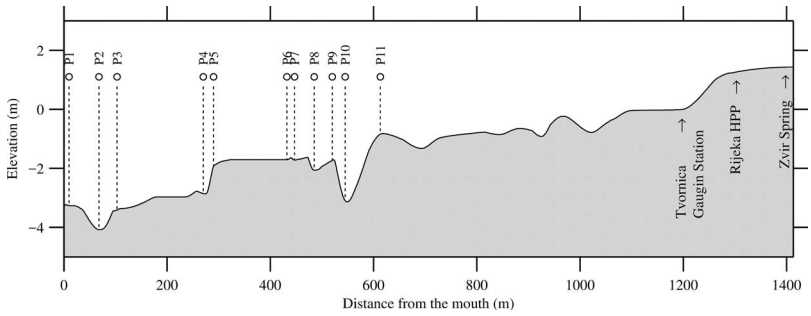

Figure 3. Longitudinal profile of the Rječina River bed elevations from the mouth to the Zvir spring.

cm by the year 2100 (IPCC, 2014). Tsimplis *et al*. (2012) used tidal gauge records from the Bakar tidal station in the Adriatic Sea to analyze trends in its sea level and estimated an increase of 3.3 ± 0.5 mm y^{-1}, indicating that the total SLR by the year 2100 could reach 33 cm. In contrast, Baric, Grbec, and Bogner (2008) examined the potential effects of a global SLR along the Croatian coast based on the assumed values between 20 cm and 86 cm. To model and predict the potential impacts of SLR, numerical models are regularly applied.

Numerical Study of Salt-Wedge Estuaries

Three-dimensional numerical models are widely used in the simulation of various dynamic estuarine processes (Mahgoub, Hinkelmann, and La Rocca, 2015; Shaha, Cho, and Kim, 2013; Xiao *et al*., 2014; Yuan, Zhu, and Wang, 2015), although their computational cost may sometimes be too great for engineering purposes. This is especially true for highly stratified estuaries, where a very fine vertical discretization is needed to adequately represent a thin interface. Three-dimensional models are necessary to realistically simulate partially or well-mixed estuaries, where their main physical properties vary in both vertical and horizontal directions. Two-layer models, however, can adequately describe all of the relevant processes operating in salt-wedge estuaries if stratification is strong enough to suppress vertical mixing and if the interfacial layer is much thinner than the upper and lower layers.

Schijf and Schönfeld (1953) and Stommel and Farmer (1952) were among the first to develop the mathematical theory for a two-layer flow in salt-wedge estuaries. Both models were based on shallow-water theory and the assumption that a salt wedge can adequately be represented by two layers of immiscible fluid, separated by a pycnocline of zero thickness. This simplification is justified by the fact that the exchange between the layers in salt wedges is minimal compared to the extent of advective processes within each layer. Early investigators mainly focused on arrested salt wedges and based their research on simple steady-state solvers (Arita and Jirka, 1987a,b; Balloffet and Borah, 1985; Dermissis and Partheniades, 1985; Grubert, 1989). Dazzi and Tomasino (1974) extended this theory and developed a one-dimensional two-layer time-dependent numerical model to study tidal dynamics in the Po River; however, although their model described the main features of the tidal flow, it neglected the convective acceleration terms in the momentum equations. Several two-layer models solving full shallow-water equations (Liu *et al*., 2015; Ljubenkov, 2015; Sierra *et al*., 2004) have been successfully applied in salt-wedge estuaries over the last few years. Although these models are valid for gradual changes in tidal and riverine flows, they are not shock capturing and thus cannot correctly describe the internally transcritical flow that may occur under highly dynamic conditions at sills and lateral channel contractions (Armi, 1986; Farmer and Armi, 1986). Recently, several studies presented and examined shock-capturing numerical models for a single-layer shallow-water flow based on a finite-volume method and a Q-scheme (Bermudez and Vázquez-Cendón, 1994; Vázquez-Cendón, 1999). Castro *et al*. (2004, 2005, 2007) extended these models and presented a general formulation for a one-dimensional (1D) two-layer exchange flow in channels with irregular geometry, which was successfully applied in a case study of the Strait of Gibraltar. Irregular and variable channel geometry can also be resolved by two-dimensional two-layer shallow-water models (*e.g.,* La Rocca *et al*., 2012a; La Rocca *et al*., 2012b). In the case of the

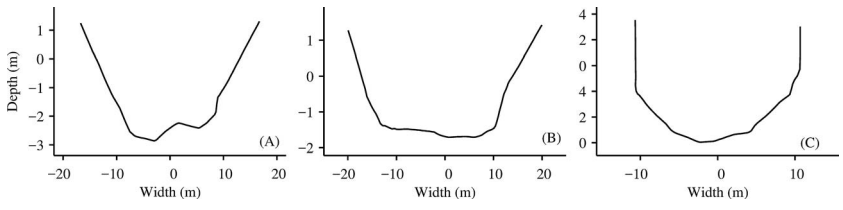

Figure 4. Characteristic cross sections of the Rječina River Estuary for (A) lower reaches (0+150), (B) middle reaches (0+325), and (C) upper reaches (0+650).

Rječina River Estuary, however, the average channel width is fairly uniform (Figures 1 and 4), and the flow is mainly unidirectional; hence, a simpler 1D model that accounts for the irregular cross sections of the channel can be considered as adequate.

Aim of This Study

Field observations and the numerical study of the salt-wedge intrusion in the Rječina River Estuary under different hydrological conditions were considered for several reasons. First, published studies of microtidal salt wedges are scarce, hence there is a clear motivation to better understand relevant physical processes, such as the stratification, salinity structure, and the salt-wedge propagation rate, in these environments. Second, the Rječina River Estuary is a very favorable field site for the validation of the numerical model developed for simulating salt-wedge dynamics. Because of a relatively short length, well-controlled inflow, and nearly negligible tidal oscillations, steady flow conditions are easily achieved, and the movement of the salt wedge is easily observed. Finally, the intrusion of the salt water may have a negative impact on the freshwater resources located in the close vicinity of the estuary, in particular Zvir spring, especially if the climate change predictions of SLR and the reduction of available freshwater are realized.

Therefore, in this study, the salinity structure, intrusion length, and shape of a salt wedge was analyzed under different hydrological conditions to examine its dynamic response to highly variable river flow rates and to better understand the implications of future SLR on the saltwater intrusion in the Rječina River Estuary.

METHODS

The following section presents the governing equations for a salt-wedge estuary alongside a corresponding numerical modeling scheme. Details of field observations made in the Rječina River Estuary are also described.

Governing Equations

The mathematical model was derived by adapting a general formulation for two-layer exchange flows in channels with irregular geometry (Castro *et al.*, 2004) to include the entrainment and shear stress at the channel bed, walls, and layer interface.

In the hydraulic sense, two-layer flows in salt-wedge estuaries are similar to exchange flows in straits or channels, though with a few notable differences. First, salt wedges are under the influence of many different forcing mechanisms, such as tidal, fluvial, and estuarine (Geyer and Ralston, 2011). Second, the upper layer in a salt-wedge estuary is usually more active than the lower one, which can be motionless or flow in the same or opposite direction. Finally, the shape of a salt wedge is more sensitive to the interfacial shear stress than the exchange flow in sea straits. Although the vertical mixing in salt-wedge estuaries is reduced by a strong stratification, it may nonetheless appear because of locally enhanced shear stress and thus should be considered in numerical models.

By accounting for the shear stress and entrainment as additional source terms in the momentum equations, the final conservative form of the governing system is written as follows:

$$\frac{\partial \mathbf{w}}{\partial t}+\frac{\partial \mathbf{f}(\boldsymbol{\sigma},\mathbf{w})}{\partial x}=\mathbf{B}(\boldsymbol{\sigma},\mathbf{w})\frac{\partial \mathbf{w}}{\partial x}+\mathbf{v}(\boldsymbol{\sigma},\mathbf{w})+\mathbf{s}(x,\boldsymbol{\sigma},\mathbf{w}), \tag{1}$$

where

$$\mathbf{w}(x,t)=\{A_1(x,t)Q_1(x,t)A_2(x,t)Q_2(x,t)\}^T, \tag{2}$$

$$\mathbf{f}(\boldsymbol{\sigma},\mathbf{w})=\begin{Bmatrix} Q_1 \\ \dfrac{Q_1^2}{A_1}+\dfrac{g}{2\sigma_1}A_1^2 \\ Q_2 \\ \dfrac{Q_2^2}{A_2}+\dfrac{g}{2\sigma_2}A_2^2 \end{Bmatrix}, \tag{3}$$

$$\mathbf{B}(\boldsymbol{\sigma},\mathbf{w})=\begin{bmatrix} 0 & 0 & 0 & 0 \\ 0 & 0 & -g\dfrac{A_1}{\sigma_1} & 0 \\ 0 & 0 & 0 & 0 \\ -g\dfrac{A_2}{\sigma_1} & 0 & 0 & 0 \end{bmatrix}, \tag{4}$$

$$\mathbf{v}(\boldsymbol{\sigma},\mathbf{w})=\begin{Bmatrix} 0 \\ \dfrac{g}{2}\dfrac{\partial}{\partial x}\left(\dfrac{1}{\sigma_1}\right)A_1^2 \\ 0 \\ \dfrac{g}{2}\dfrac{\partial}{\partial x}\left(\dfrac{1}{\sigma_2}\right)A_2^2 \end{Bmatrix}, \tag{5}$$

and g is gravitational acceleration, A_j is the cross-sectional area, Q_j is flow rate, σ_j is the channel breadth, and index $j=1$, 2 refers to the upper and lower layer, respectively. The source term $\mathbf{s}$ accounts for varying geometry ($\mathbf{s}_G$), shear stress ($\mathbf{s}_F$), and entrainment ($\mathbf{s}_E$) as follows:

$$\mathbf{s}(x,\boldsymbol{\sigma},\mathbf{w})=\mathbf{s}_G(x,\boldsymbol{\sigma},\mathbf{w})+\mathbf{s}_F(x,\boldsymbol{\sigma},\mathbf{w})+\mathbf{s}_E(x,\boldsymbol{\sigma},\mathbf{w}), \tag{6}$$

$$\mathbf{s}_G(x,\boldsymbol{\sigma},\mathbf{w})=\begin{Bmatrix} 0 \\ gA_1\left[\dfrac{1}{\sigma_1}\dfrac{\partial}{\partial x}(A_1+A_2)-\dfrac{\partial}{\partial x}(b+h_2+h_1)\right] \\ 0 \\ gA_2\left[\dfrac{1}{\sigma_2}\dfrac{\partial A_2}{\partial x}+\dfrac{r}{\sigma_1}\dfrac{\partial A_1}{\partial x}-\dfrac{\partial}{\partial x}(b+h_2+rh_1)\right] \end{Bmatrix}, \tag{7}$$

$$\mathbf{s}_F(x,\boldsymbol{\sigma},\mathbf{w})=\begin{Bmatrix} 0 \\ \dfrac{\tau_w}{\rho_1}O_1'+\dfrac{\tau_i}{\rho_1}\sigma_3 \\ 0 \\ \dfrac{\tau_b}{\rho_2}O_2-\dfrac{\tau_i}{\rho_2}\sigma_3 \end{Bmatrix}, \tag{8}$$

$$\mathbf{s}_E(x,\boldsymbol{\sigma},\mathbf{w})=\begin{Bmatrix} \sigma_3 w_e \\ \sigma_3 u_1 w_e \\ -\sigma_3 w_e \\ -\sigma_3 u_2 w_e \end{Bmatrix}, \tag{9}$$

where O_j is the wetted perimeter, u_j is water velocity, b is bed elevation, h_j is layer depth, r is the ratio between the upper (ρ_1) and lower (ρ_2) density, τ_w is wall shear stress in the upper layer, τ_b is bed shear stress in the lower layer, τ_i is shear stress at the interface between the layers, and w_e is entrainment velocity. Here, the entrainment defines only the vertical transport of fluid volume from a more active layer to a less active layer, and the density of each layer remains constant (*i.e.* $\rho_i(x, t) = \text{const.}$). This simplification can be justified by the assumption that vertical mixing in highly stratified fluids is mostly confined to the interfacial layer, with it imparting a very weak influence on the density structure of either the upper or lower layer.

Numerical Scheme

The numerical techniques presented by Castro *et al*. (2004, 2005, 2007) were used to solve Equation (1). It is important to note that Equation (1) has nonconservative terms; however, this system can be interpreted as

$$\frac{\partial \mathbf{w}}{\partial t} + A(\boldsymbol{\sigma}, \mathbf{w})\frac{\partial \mathbf{w}}{\partial x} = \mathbf{s}(x, \boldsymbol{\sigma}, \mathbf{w}), \tag{10}$$

where $\mathcal{A}$ is a matrix defined as $\mathcal{A}(\boldsymbol{\sigma}, \mathbf{w}) = \mathrm{J}(\boldsymbol{\sigma}, \mathbf{w}) - B(\boldsymbol{\sigma}, \mathbf{w})$, with

$$\mathrm{J}(\boldsymbol{\sigma}, \mathbf{w}) = \begin{pmatrix} 0 & 1 & 0 & 0 \\ -\dfrac{Q_1^2}{A_1^2} + \dfrac{g}{\sigma_1}A_1 & 2\dfrac{Q_1}{A_1} & 0 & 0 \\ 0 & 0 & 0 & 1 \\ 0 & 0 & -\dfrac{Q_2^2}{A_2^2} + \dfrac{g}{\sigma_2}A_2 & 2\dfrac{Q_2}{A_2} \end{pmatrix}. \tag{11}$$

Therefore, as shown by Castro *et al*. (2004), Roe's method based on the approximate Riemann state solver, can be applied to solve Equation (1). The numerical scheme is based on a finite-volume method: a generalized Q-scheme of Roe for the flux terms and an upwind scheme for the source terms (Vázquez-Cendón, 1999). The model is explicit in time, shock capturing, and satisfies the extended conservation property for water at rest. The importance of upwinding the source terms, accounting for bed slope, and varying geometry was demonstrated by Bermudez and Vázquez-Cendón (1994). A similar upwind treatment of friction terms in channels with rectangular cross sections was proposed by Rebollo, Delgado, and Fernández-Nieto (2003). Likewise, Cea *et al*. (2004) showed that mass terms such as lateral inflows or entrainment (as is relevant herein) should also be upwinded to reduce discretization errors introduced by upwinding the flux terms and to ensure the stability of the numerical scheme. The proposed numerical scheme for solving a two-layer exchange flow was thoroughly validated against approximate stationary analytical solutions of maximal two-layer exchange flows through simplified channels (Castro *et al*., 2004; Castro, Macias, and Pares, 2001). Furthermore, Castro *et al*. (2007) assessed the performance of such a model for the exchange flow through realistic geometry of the Strait of Gibraltar.

The spatial domain in the model was initially divided into M control volumes or cells. If cells of equal size are assumed, then their dimensions can be denoted by $\Delta x = x_{i-1/2} - x_{i+1/2}$, although this method is also applicable to irregular meshes. The time step was denoted by Δt, the number of time steps by n, such that the total simulation time was $n\Delta t$. The explicit numerical schemes require that Δx and Δt satisfy the Courant-Friedrichs-Lewy (CFL) condition to be stable. In this numerical scheme the following condition had to be satisfied:

$$\frac{\Delta \mathrm{t}}{\Delta x}\max(|\lambda_{i+1/2,l}|) \le \mathrm{CFL}, \tag{12}$$

where $\lambda_{i+1/2,l}$ are eigenvalues of matrix $\mathcal{A}$, $0 < \mathrm{CFL} \le 1$, $0 \le \mathrm{l} \le 4$, and $0 \le i \le M$.

A common difficulty encountered in this type of model is resolving the tip of the salt wedge, which is a lower-layer wet–dry front. A tolerance parameter ε was defined to avoid instabilities and negative depths. When the lower layer depth $h_2 < \varepsilon$, the cell was considered to be wetted only by the upper layer, the lower-layer velocity was set to zero ($u_2 = 0$); however, h_2 remained unchanged to preserve the mass-conservation property of the scheme. Furthermore, the source term accounting for bed elevation in the lower layer was redefined near steep bed slopes following the procedure described in Castro *et al*. (2005).

Boundary Condition

In arrested salt-wedge models, it is usually assumed that the flow in the upper layer is critical at the river mouth (Balloffet and Borah, 1985; Schijf and Schönfeld, 1953). In time-dependent models, however, both layers are active, and the critical flow should be described by a composite Froude number G (Pawlak and Armi, 1997):

$$G^2 \cong \mathrm{F}_1^2 + F_2^2 = 1, \tag{13}$$

and

$$F_1^2 = \frac{Q_1^2\sigma_1}{g(1-r)A_1^3}\frac{\sigma_3}{\sigma_2}, \quad F_2^2 = \frac{Q_2^2\sigma_3}{g(1-r)A_2^3}, \tag{14}$$

where F_1 and F_2 are internal Froude numbers for the upper and lower layer, respectively, when irregular cross sections are considered. It can be problematic to determine the exact position of the mouth in salt-wedge estuaries because of the irregular channel geometry; however, Farmer and Armi (1986) showed that two-layer flows may involve an internally critical flow (a hydraulic control point) located where strong lateral contractions are present, which are more easily identified. Krvavica *et al*. (2012) examined the hydraulic conditions in the Rječina River Estuary and found that a hydraulic control point is located at the bridge nearest to the mouth (Figure 1: point P1), which was thus used herein as a downstream boundary.

Shear Stress and Entrainment

The bed, wall, and interfacial shear stresses in Equation (8) were defined by a quadratic law and friction factors:

$$\tau_b = -\rho_2\lambda u_2|u_2|, \tag{15}$$

$$\tau_w = -\rho_1\lambda u_1|u_1|, \tag{16}$$

$$\tau_i = -\frac{\rho_1 + \rho_2}{2}\lambda_i(u_1 - u_2)|u_1 - u_2|. \quad (17)$$

The bed and wall-friction factor λ, equal to one-eighth of the Darcy–Weisbach factor (f), was calculated using a modified explicit Colebrook–White formula for open channels (Yen, 2002):

$$\lambda = \frac{1}{32}\left[-\log\left(\frac{k_s}{12R} + \frac{1.95}{\mathrm{Re}^{0.9}}\right)\right]^{-2}, \quad (18)$$

where k_s is bed roughness height, $R = A/O$ is hydraulic radius, $\mathrm{Re} = (u_1 R_1)/\upsilon$ is the Reynolds number, and υ is kinematic viscosity. The interfacial friction factor λ_i was calculated using an empirical formula derived from observations at the Rječina River Estuary by Krvavica, Travaš, and Ožanić (2016):

$$\lambda_i = (8.9 \times 10^5 \mathrm{Re} Ri^3)^{-2}, \quad (19)$$

where $Ri = g(\rho_1 h_1)/(\Delta\rho \Delta u^2)$ is the bulk Richardson number.

The entrainment velocity (w_e) is defined by the entrainment rate $E = w_e/(u_1 - u_2)$, which was computed using the formula based on field observations by Pedersen (1980) in several estuaries and fjords:

$$E = 1.5 \times 10^{-3} Ri^{-2}. \quad (20)$$

Field Observations

Field observations in the Rječina River Estuary were performed during the period from February to September 2014 and from April to August 2015. Thirty sampling campaigns covered various hydrographic conditions, with sea levels ranging from –0.5 to +0.75 m a.s.l. and river flow rates (Q) in the range from 1.3 to 29.8 $\mathrm{m^3\ s^{-1}}$. For this range of flow rates, the salt wedge was always present in the estuary ($Q < 38.1\ \mathrm{m^3\ s^{-1}}$). Eleven sampling points were selected along the estuary (Figure 3), with most of them located at bridges traversing it. Vertical profiles of salinity (S) and temperature (T) were measured by a Schlumberger conductivity-temperature-depth diver. Density profiles were computed from the measured S–T data based on empirical equations (Fofonoff and Millard, 1983). River flow rate (Q) was either computed from a rating curve or measured directly by a Teledyne StreamPro acoustic Doppler current profiler (ADCP) positioned upstream from the salt wedge. Only observations made under steady-state conditions were considered (*i.e.* an arrested salt wedge), which were identified by Q being constant for several hours before and after the measurements, with minimal influence of wind or waves. The changes in the tidal-driven sea levels during the measurements were under 3–4 cm.

An additional sampling campaign, conducted on 1 July 2015, provided more details of the salt-wedge response to changes in the river flow rate caused by variable discharges from the Rijeka HPP. This observation differed from previous ones for several reasons. First, the propagation of the salt wedge (*i.e.* time-dependent changes in the shape of the salt wedge) was observed in contrast to the stationary, arrested salt-wedge shape; second, the vertical S–T profiles were measured continuously along the estuary every 10–15 minutes during a period of 12 hours, in contrast to only one measurement along the wedge for the arrested salt wedge; and finally, a Nortek Aquadopp Profiler ADCP was positioned near the river mouth to measure the vertical velocity profiles. River flow rate (Q) was measured by a combination of water-gauge data, rating curves, and a Teledyne StreamPro ADCP located upstream from the salt wedge.

Several characteristic salinity and velocity profiles obtained from near the river mouth for different flow rates are presented in Figure 5. Velocity profiles obtained under steady-state conditions are characterized by a nearly stagnant lower layer and a characteristic turbulent logarithmic shape in the upper layer; Figures 5A and B show S-u profiles for $Q_1 = 9.7\ \mathrm{m^3\ s^{-1}}$ and $Q_1 = 13.3\ \mathrm{m^3\ s^{-1}}$, respectively. During a decrease in Q, the salt wedge advanced upstream, which resulted in negative velocities in the lower layer, *i.e.* return flow; Figure 5C shows the S-u profile for $Q_1 = 6.5\ \mathrm{m^3\ s^{-1}}$ and $Q_2 = -1.1\ \mathrm{m^3\ s^{-1}}$. Figure 5D shows the velocity profile of a salt wedge receding toward the river mouth during an increase in Q, as characterized by positive velocities in the lower layer ($Q_1 = 12.0\ \mathrm{m^3\ s^{-1}}$ and $Q_2 = 2.1\ \mathrm{m^3\ s^{-1}}$). All salinity profiles show a sharp halocline, suggesting that a very stable and strong vertical stratification was present under all conditions. To quantify the strength of the stratification, a squared buoyancy frequency (N^2), or Brunt–Väisälä frequency, was computed at each sampling point using the following equation:

$$N^2(h_i) = \frac{g}{\rho_i}\frac{\partial \rho}{\partial h}, \quad (21)$$

where ρ_i is density at depth h_i. The maximum value of N^2 at each transect was used as a measure of the stratification strength.

Model Validation

The model performance was assessed by comparing the numerical results against the field observations. For each arrested salt-wedge case, the model was validated by comparing the computed and observed interface depths along the estuary, whereas for the dynamic salt-wedge case, in addition to the interface depths along the estuary at multiple time steps, the flow rates per unit width in each layer, near the mouth, were also compared against field observations for the entire length of the simulation. Three skill metrics were used to quantify the agreement between the data: the mean absolute error (MAE), the correlation coefficient (CC), and the skill score (SS) (Murphy, 1988):

$$\mathrm{MAE} = \frac{1}{N}\sum |X_{\mathrm{mod}} - X_{\mathrm{obs}}|, \quad (22)$$

$$\mathrm{CC} = \frac{\sum (X_{\mathrm{mod}} - X_{\mathrm{mod}})(X_{\mathrm{obs}} - X_{\mathrm{obs}})}{\sqrt{\sum (X_{\mathrm{mod}} - X_{\mathrm{mod}})^2 \sum (X_{\mathrm{obs}} - X_{\mathrm{obs}})^2}}, \quad (23)$$

$$\mathrm{SS} = 1 - \frac{\sum (X_{\mathrm{mod}} - X_{\mathrm{obs}})^2}{\sum (X_{\mathrm{obs}} - X_{\mathrm{obs}})^2}, \quad (24)$$

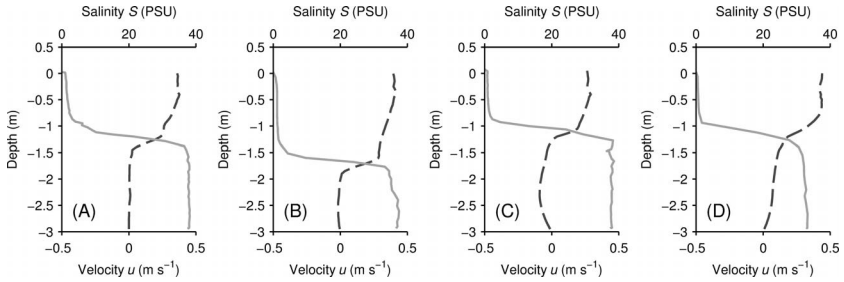

Figure 5. Characteristic salinity S (solid line) and velocity u (dashed line) profiles observed in the Rječina River Estuary for different river flow rates: (A) and (B) steady-state conditions ($Q_1 = 9.7$ m^3 s^{-1} and $Q_1 = 13.3$ m^3 s^{-1}, respectively, and $Q_2 = 0.0$ m^3 s^{-1}), (C) the salt wedge advanced upstream ($Q_1 = 6.5$ m^3 s^{-1} and $Q_2 = -1.1$ m^3 s^{-1}), and (D) the salt wedge receded downstream toward the river mouth ($Q_1 = 12.0$ m^3 s^{-1} and $Q_2 = 2.1$ m^3 s^{-1}).

where N is the number of data points, X_{mod} is modeled data, X_{obs} is observed data, and the overbar represents a mean value. A perfect correlation is indicated by MAE = 0, CC = 1, and SS = 1, whereas large values of MAE, CC = 0, and SS = 0 indicate no correlation.

RESULTS

The results obtained from both numerical simulations and field observations are presented in this section. The intrusion length and salinity structure of the salt wedge under steady state and highly variable riverine conditions were examined. In both cases, the performance of the numerical model was analyzed by comparing the solutions to the field observations. Finally, the impact of SLR on salt-wedge intrusion in the Rječina River Estuary was assessed.

Intrusion Length and Salinity Structure of the Arrested Salt Wedge

The numerical model was applied to compute the interface depths along the Rječina River Estuary under steady flow conditions. The model domain was discretized by $M = 108$ cells, with the spatial step $\Delta x = 10$ m and temporal step $\Delta t = 0.5$ s, to satisfy the CFL condition. Density ratios were set on a case-by-case basis according to the measured upper and lower layer densities and ranged from 0.972 to 0.976. The upstream and downstream boundary conditions were defined by a constant river flow and by a hydraulic control condition and constant total depth at the mouth, respectively. Five outcomes are presented here, which are representative of a total of 30 simulations performed.

The computed and observed shapes of the arrested salt wedge are shown in Figure 6. In general, for a higher freshwater flow rate, the arrested salt-wedge length was shorter, and the interface was deeper in the channel. The intrusion length was also influenced by sea level; for example, a longer salt-wedge length was observed for $Q = 6.5$ m^3 s^{-1} in comparison to $Q = 4.2$ m^3 s^{-1}, attributable to a higher sea level in the former (Figure 6). The variable slope of the interface was mainly the result of the irregular channel geometry in the estuary. The length of the arrested salt wedge and the slope of the interface were also seen to be sensitive to the interfacial friction factor λ_i, which needed to be chosen carefully to obtain satisfactory agreement with field observations; thus, the empirical Equation (19), which was obtained by fitting the numerical solutions against field observations, was used herein. Comparing the numerical solutions with field observations assessed the model performance: Overall, all skill metrics indicated a strong agreement between the modeled and observed interface shapes, with an MAE of 0.12 m, a CC of 0.94, and a SS of 0.87 (Table 1).

The observed mean densities in both layers and maximum squared buoyancy frequencies (N^2) are also presented in Figure 6. Longitudinal variations in densities were negligible in all considered cases, with typical observed values of $\rho_1 = 1001 \pm 3$ kg m^{-3} in the upper layer and $\rho_2 = 1026 \pm 2$ kg m^{-3} in the lower layer. N^2 varies slightly along the wedge, probably because of local irregularities in the channel geometry, rather than any along-wedge stratification variability. A very high average value of $N^2 \approx 1.0$ indicates that a highly stratified structure is preserved under constant river flow rate, regardless of sea level or tidal dynamics.

Response of the Salt Wedge to Changes in the River Flow Rate

The response of a salt wedge in the Rječina River Estuary to changes in the river flow rate was examined both numerically and through field observations. Krvavica *et al.* (2012) showed that the flow rate in the lower reaches of the Rječina River during summer months is highly sensitive to discharges from the Rijeka HPP. On 1 July 2015, the Rijeka HPP started and stopped on two occasions in an 8-hour period (from 0700 to 1500), which caused highly dynamic conditions to form in the estuary, and the river flow rate ranged from 4.2 m^3 s^{-1} to 13.9 m^3 s^{-1}.

For numerical modeling of this scenario, a denser mesh was chosen to accurately address highly dynamical conditions; the domain setup comprised $M = 216$, $\Delta x = 5$ m, and $\Delta t = 0.25$ s to satisfy the CFL condition. The density ratio $r = \rho_1/\rho_2$ was set to 0.975, corresponding to the observed freshwater ($\rho_1 = 1000$ kg m^{-3}) and saltwater ($\rho_2 = 1026$ kg m^{-3}) densities. The upstream and downstream boundary conditions were forced by the observed river hydrograph (Figure 7A) and by the hydraulic control condition (Equation [13]) and a total depth corresponding to the observed sea levels (Figure 7B), respectively. The numerical simulation started at 0720 and lasted until 1540 (500 min) to capture all the changes in the salt-wedge shape (at

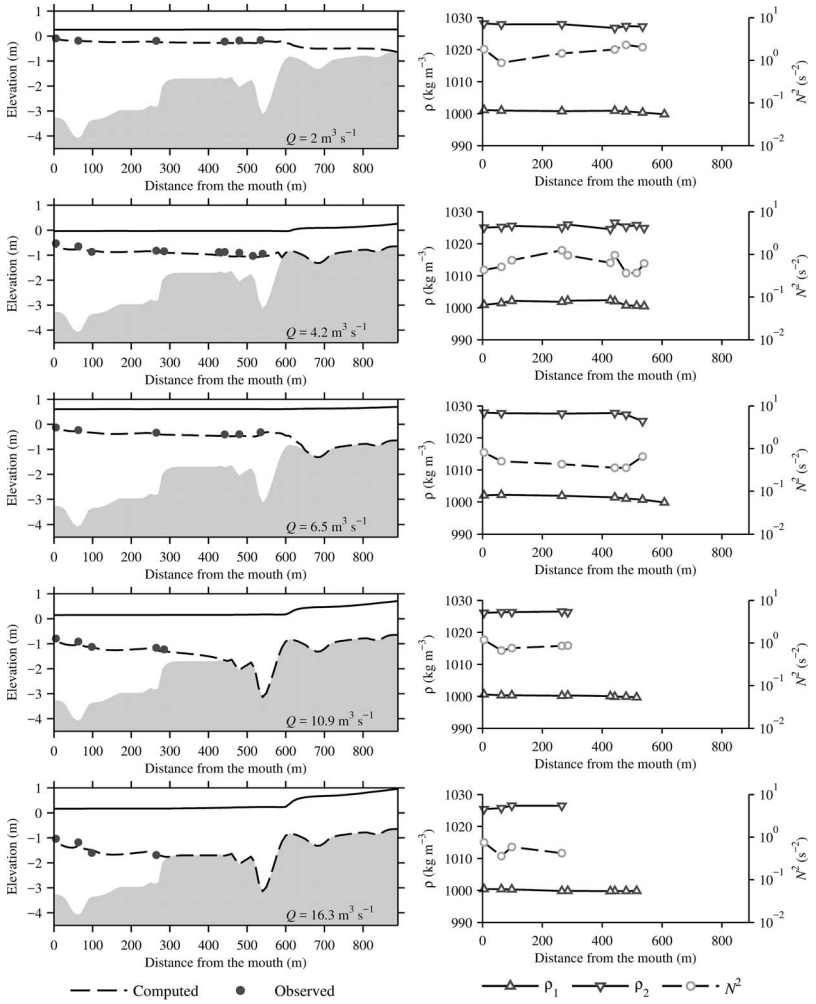

Figure 6. Longitudinal profiles of the Rječina River Estuary with computed and observed interface depths shown on the left panel and observed average densities in the lower (ρ_2) and upper (ρ_1) layers with maximum squared buoyancy frequencies (N^2) shown on the right.

1540 the conditions in the estuary became stationary and the arrested salt wedge was formed).

The computed and observed interface depths along the estuary are presented in Figure 8. Both numerical solutions and field observations showed that the salt wedge responded almost instantly to changes in the river flow rate by moving along the estuary in either an upstream or downstream direction. When Q increased, the salt wedge receded downstream toward the mouth, and vice versa.

Table 1. *Mean absolute error (MAE), correlation coefficient (CC), and skill score (SS) for each comparison of the computed and observed interface depths and flow rates per unit width described in the main text.*

	Steady State	Time Dependent		
	Interface Depth	Interface Depth	Flow Rate per Unit Width	
	h_1 (m)	h_1 (m)	q_1 (m^2 s^{-1})	q_2 (m^2 s^{-1})
MAE	0.12	0.12	0.018	0.014
CC	0.94	0.9	0.99	0.95
SS	0.87	0.8	0.97	0.89

The computed and observed flow rates per unit width (q_i) in each layer were also analyzed (Figure 9). Near the river mouth, q_1 varied proportionally to Q; however, q_2 seemed to respond more to the movement of the salt wedge than to the freshwater flow rate. When Q increased, q_2 indicated a flow in the downstream direction. Similarly, when Q decreased, q_2 indicated a flow in the upstream direction. In both cases, after an equilibrium condition was reached (*i.e.* an arrested salt wedge was established), q_2 returned to near-zero values.

All skill metrics indicated a strong agreement between the modeled and observed data. For h_1, the MAE was 0.12 m, the CC was 0.9, and the SS was 0.8 (Table 1). For q_1, the MAE was 0.018 m^2 s^{-1}, the CC was 0.99, and the SS was 0.97; for q_2, the MAE was 0.014 m^2 s^{-1}, the CC was 0.95, and the SS was 0.89 (Table 1).

To assess the salinity structure of the salt wedge under the influence of a variable Q, both the observed densities in the

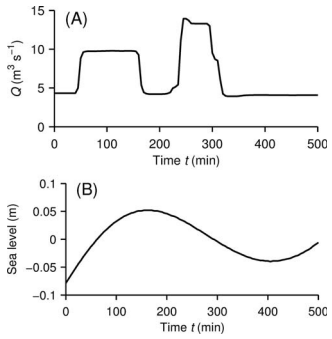

Figure 7. Boundary conditions: (A) upstream river hydrograph and (B) downstream sea level.

upper and lower layers and the maximal observed squared buoyancy frequencies were averaged along the estuary at each time step. All three parameters are shown in Figure 10. The longitudinal salinity structure was similar, as in the case of an arrested salt wedge, and the overall layer densities remained nearly constant during the simulation. Furthermore, the buoyancy frequency indicated that a strong stratification was persistent during the simulation, with maximum values ranging from 0.4 to 1.0 s^{-2}.

Impact of SLR on Saltwater Intrusion in the Rječina River Estuary

The impact of SLR on saltwater intrusion in the Rječina River Estuary was examined by considering different tidal levels, SLR scenarios, and low-flow rates. Long-term mean sea level (MSL) at the Bakar tidal gauging station is +0.11 m a.s.l., and mean higher high water (MHHW) is +0.72 m a.s.l. (Rezo and Pavasović, 2014). Different studies of SLR (Baric, Grbec, and Bogner, 2008; IPCC, 2014; Tsimplis *et al.*, 2012)

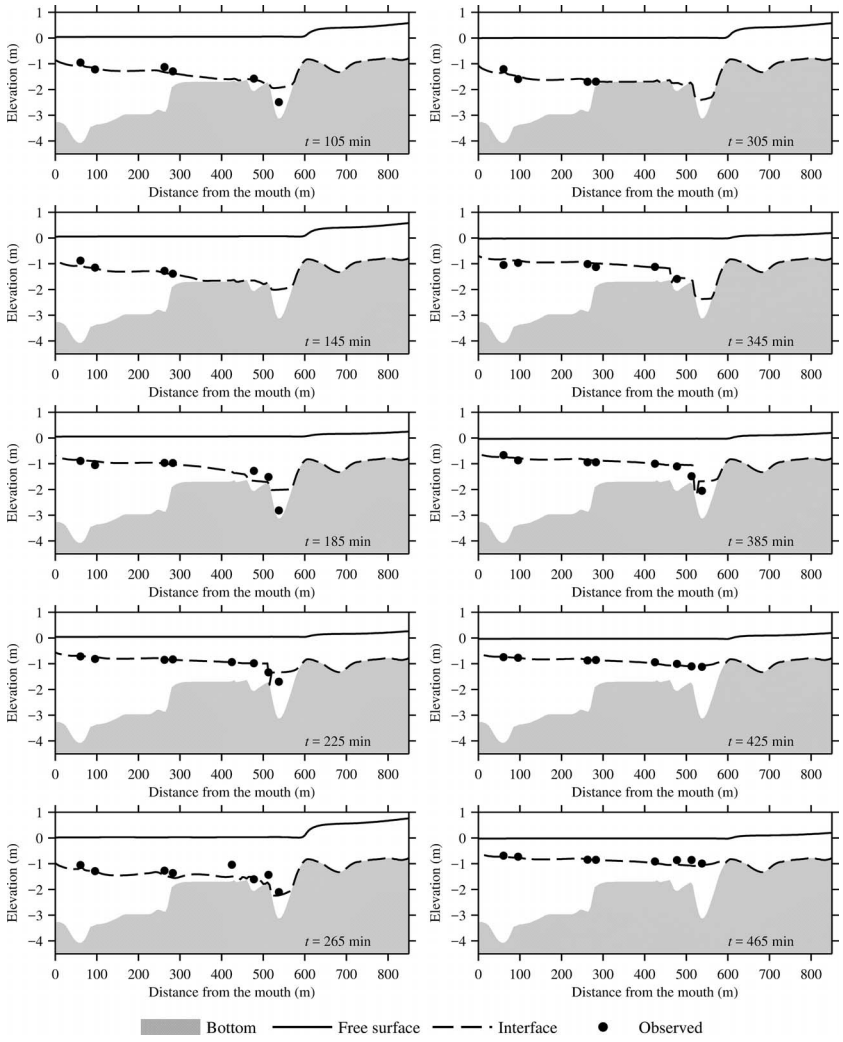

Figure 8. Longitudinal profiles of the Rječina River Estuary with the computed and observed changes of interface depths during a variable river flow.

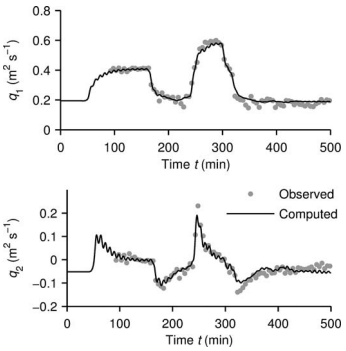

Figure 9. Computed and observed changes of flow rates per unit width in the upper (q_1) and lower (q_2) layers for a variable river flow case.

suggest different rates of change over a range of spatial and temporal scales, although for this study two projected global SLR values for the year 2100 were assumed: a realistic +33 cm and an extreme +80 cm. Therefore, salt-wedge intrusion was examined for six seawater-level (SWL) scenarios: (1) present MSL (+0.11 m a.s.l.), (2) present MHHW (+0.72 m a.s.l.), (3) MSL and a realistic SLR (+0.44 m a.s.l.), (4) MHHW and a realistic SLR (+1.05 m a.s.l.), (5) MSL and an extreme SLR (+0.91 m a.s.l.), and (6) MHHW and an extreme SLR (+1.52 m a.s.l.).

When negative impacts of climate change on coastal and estuarine ecosystems are assessed, both the SLR and the freshwater quantity should be considered. In addition to the Rječina River mean flow rate ($Q = 10.9$ m^3 s^{-1}), three low-flow indices were chosen and combined with the SWL scenarios: (1) a mean monthly average for August ($Q = 3.07$ m^3 s^{-1}), (2) a mean monthly minima for August ($Q = 1.46$ m^3 s^{-1}), and (3) a 95-percentile exceedance flow rate ($Q = 0.62$ m^3 s^{-1}). Unfortunately, no analysis of the climate change impact on the water availability in the Rječina catchment is available, and it is outside the scope of this study; however, similar studies investigating the climate change impacts on other karst springs in the northern Adriatic are available in the literature. For example, in nearby Istria County, different climate models were applied to predict changes in the precipitation, temperature, and the water availability at several karst springs for the future period 2021–50 (Karleuša

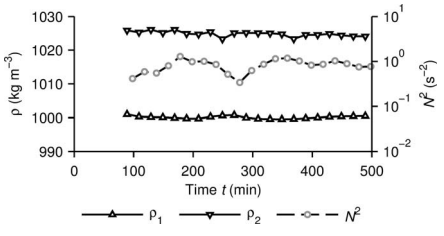

Figure 10. Observed averaged densities in the lower (ρ_2) and upper (ρ_1) layers and maximum squared buoyancy frequency (N^2) for a variable river flow case.

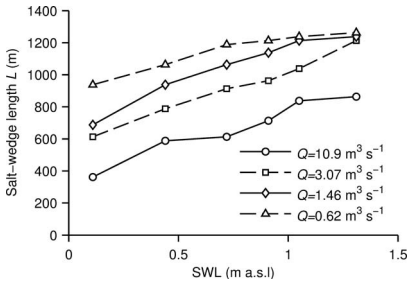

Figure 11. The intrusion length (L) in the Rječina River Estuary for different sea levels (SWL) and river flow rates (Q).

et al., 2016). These assessments indicated that more extremely dry years are expected and that a minimum mean monthly flow, for example, at Gradole spring, is expected to decrease by 5.6%–13.1%, depending on the climate model used. These studies suggest that a similar decrease in minimum flow and longer dry periods may also be expected for Zvir and Rječina springs.

To predict the impact of SLR on the maximum salt-wedge intrusion, the model domain was defined by $M = 140$, $\Delta x = 10$ m, and $\Delta t = 0.5$ s, with $r = 0.975$ (after typical freshwater and saltwater densities of 1000 kg m^{-3} and 1026 kg m^{-3}, respectively). The upstream and downstream boundary conditions were forced by a combination of the six sea-level scenarios and constant river flows, as previously defined. The simulation ended when a steady state was reached (*i.e.* $dQ_1/dt = 0$).

Computed intrusion lengths (L) are shown in Figure 11. The minimal $L = 360$ m is predicted for the present MSL (+0.11 m) and the mean flow rate ($Q = 10.9$ m^3 s^{-1}), while the maximum $L = 1263$ m is predicted for MHHW with an extreme SLR (+1.52 m) and the 95-percentile exceedance flow rate ($Q = 0.62$ m^3 s^{-1}). Both the river flow rate and sea level affect the intrusion length equally for high Q values, although sea level and channel geometry appear to be more influential for low Q values. The maximum intrusion length of the salt wedge was limited to 1300 m because of a channel bed step, located just upstream of the Tvornica gauging station. This step is ~1 m high and acts as a weir during low to medium river flow rates, thus preventing the salt-wedge front from advancing upstream (Figure 3).

In general, the salt-wedge intrusion length follows a power-law relationship with the river flow rate ($L \sim Q^n$). For example, Ralston *et al.* (2010) found coefficient $n = -0.19$ for low-flow conditions in the Merrimack River Estuary, and Monismith *et al.* (2002) obtained $n = -0.14$ in San Francisco Bay; however, in the Rječina River Estuary, L depends not only on Q but also on the SWL. Therefore, the following nonlinear equation was obtained (CC = 0.94):

$$L = 775.9Q^{-0.27} + 403.4\text{SWL}. \quad (25)$$

Thus, this simple equation can be used for preliminary assessment of the intrusion length in the Rječina River Estuary if the river flow rate and the sea level are known.

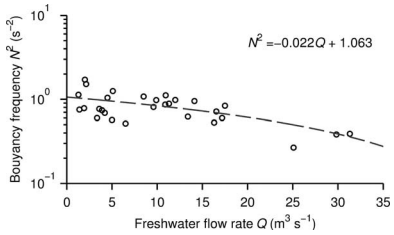

Figure 12. The observed maximum squared buoyancy frequencies (N^2) averaged along the salt wedge for different river flow rates (Q).

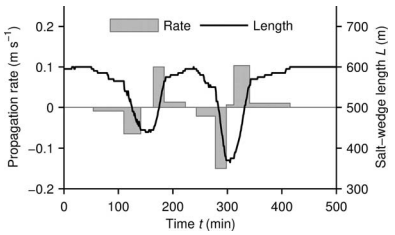

Figure 13. Computed movement of the salt-wedge front and corresponding propagation rates during a variable river flow observed on 1 July 2015.

DISCUSSION

The previous results, when considered together with the specific features of a microtidal salt-wedge estuary, lead to two interesting points that deserved additional discussion: the influence of the river flow rate on stratification and the propagation rate of the salt-wedge front.

Stratification in a Microtidal Salt Wedge

Stratification strength in the Rječina River Estuary was estimated based on a maximum squared buoyancy frequency, which showed relatively high values for all studied conditions. Geyer, Scully, and Ralston (2008) reported typical values for N^2 ranging from 0.0025–0.01 s^{-2} for partially mixed estuaries and up to $N^2 = 0.1$ s^{-2} for salt-wedge estuaries. Peters (1997) found that N^2 sometimes approached 0.1 s^{-2} in the Hudson River Estuary, with a similar upper limit also observed in the Columbia River by Kay and Jay (2003). In the Rječina River Estuary, however, the observed N^2 values ranged from 0.27 s^{-2} up to 1.71 s^{-2}, which is over one order of magnitude larger than any value reported from other field studies. Furthermore, it seems that in the absences of tides, Q has a negative influence on the stratification. This is expected, however, as turbulence produced at the channel bed or the layer interface may also induce vertical mixing (Stacey, Rippeth, and Nash, 2011). As Q increases, the shear stress exerted on the interface becomes more intense, the interfacial instabilities start to develop, and vertical mixing can begin. In this case, a high Q actually diffuses the interface layer and weakens the stratification. In the Rječina River Estuary, it was found that N^2 subsides with a higher freshwater flow rate until the salt wedge is expelled from the estuary (Figure 12).

The buoyancy frequency in the Rječina River Estuary varied slightly from 0.34 s^{-2} up to 1.28 s^{-2} under variable river flow rates (Figure 10). During the rising flow, the salt-wedge front receded toward the river mouth, and the interface layer became more diffused, which weakened the stratification. After the salt wedge receded, a force equilibrium was established, and highly stratified conditions were quickly restored. On the other hand, during the falling river flow, the salt-wedge front advanced upstream, but the stratification was unaffected. A similar mechanism was observed in the Columbia River Estuary during different tidal phases by Kay and Jay (2003), who found that during the ebb tides when the salt-wedge front receded, the shear stress at the interface induced the turbulent mixing, which weakened the stratification, but strong longitudinal density gradients quickly restored the salinity structure. During the flood tides, when the salt-wedge front advanced upstream, the shear stress at the channel bed was the dominant source of turbulence; however, it was limited to the lower layer and had little or no effect on the overall stratification.

The Propagation Rate of the Salt-Wedge Front

Based on the simulation performed for the variable river flow observed on 1 July 2015, the changes in intrusion length are plotted in Figure 13 to allow a more detailed examination of the salt-wedge propagation rates. The length of the salt wedge varied during the simulation between 600 m for the lowest Q (4.3 $m^3 s^{-1}$) and 375 m for the highest Q (13.9 $m^3 s^{-1}$). Based on this salt-wedge movement along the estuary, the propagation rates of the salt-wedge front were also computed (Figure 13). During the first wave, when Q increased from 4.3 $m^3 s^{-1}$ to 9.8 $m^3 s^{-1}$, the salt-wedge front receded at a rate of –0.06 m s^{-1}. When Q decreased back to 4.2 $m^3 s^{-1}$, the salt-wedge front advanced upstream at a rate of 0.1 m s^{-1}. Similarly, during the second wave, when Q increased to 13.9 $m^3 s^{-1}$, the salt-wedge front receded at a rate of –0.15 m s^{-1}, and when Q decreased back to 4.1 $m^3 s^{-1}$, the salt-wedge front advanced at a rate of 0.1 m s^{-1}.

These data clearly show that the rate at which the salt-wedge front moved toward the mouth was positively correlated with the river flow rate (*i.e.* the higher the increase in the river flow rate, the higher the propagation rate); however, this was not true for the upstream salt-wedge front propagation rate, which was nearly the same in both cases. A parallel can therefore be made with the propagation rate of a salt-wedge front during ebb and flood tides. Indeed, Geyer and Farmer (1989) showed that the advancement of the salt-wedge front in the Fraser River attributable to flood tides is mainly influenced by the shear stress at the channel bed. They computed that the salt-wedge front advanced at a rate of 0.7 m s^{-1}, which is a few times larger than the values in the Rječina River Estuary. Clearly, though, this comparison can be made only qualitatively because of the different driving forces involved: river flow in the Rječina River and tides in the Fraser River.

CONCLUSIONS

Field observations and numerical modeling results suggest that the Rječina River Estuary is a typical example of a microtidal salt-wedge estuary. Tidal dynamics are not strong enough to cause any significant mixing between freshwater and saltwater layers, and a highly stratified water column is

persistent for all considered flow conditions. The numerical results showed good agreement with field observations when computing the shape of the arrested salt wedge. These data showed that the intrusion length depends mainly on the river flow rate, with the MSL and channel geometry imparting second-order controls. Field observations confirmed that densities in both layers showed no significant variations along the wedge, and the observed values of squared buoyancy frequency (close to 1.0) are among the highest ever reported in a field study. Furthermore, it seems that an increase of the river flow may have a negative influence on the stratification; as Q increases, so does the shear velocity at the interface, vertical mixing is intensified, interface thickness grows and the stratification is weakened.

For highly variable flow conditions, the numerical results showed a very good agreement with field observations of interface depths, movement of the salt-wedge front, and flow rates per unit width in the upper and lower layers. Both datasets confirmed that the salt wedge reacted almost instantaneously to the changes in the river flow rate, whereby the salt-wedge front moved along the estuary until force equilibrium was achieved and an arrested salt wedge formed. The propagation rate of the salt-wedge front was proportional to the river flow rate increase when the salt wedge was receding, although the propagation rate seemed to be independent of the river flow rate when the salt wedge moved upstream. Stratification remained strong even for these highly dynamic conditions, and longitudinal density variations were negligible in both layers. Although showing very high values, the buoyancy frequency varied only slightly depending on the changes in the river flow rate. An increasing flow rate exerted a higher shear stress on the interface, which caused vertical mixing and weakened the stratification, whereas the thickness of the interfacial layer remained unchanged for a decreasing flow rate. A similar behavior has been reported in salt wedges under the influence of flood and ebb tides.

The proposed numerical model was also used to predict the impact of potential future SLR. Several scenarios were considered, which used different combinations of sea-level increase and river flow rate. The model predicted that SLR would cause a noticeable increase in the salt-wedge intrusion length; however, the step in the channel bed, located just upstream from Tvornica gauging station, would prevent the salt wedge from advancing beyond this point, even in the most unfavorable scenario. Based on these predictions, a simple equation was derived for the preliminary assessment of the salt-wedge intrusion length, which can be applied in any scenario where the river flow rate and SLR are known.

ACKNOWLEDGMENTS

This work has been supported in part by the Ministry of Science, Education, and Sports of the Republic of Croatia under the project Hydrology of Sensitive Water Resources in Karst (114-0982709-2549) and Research Infrastructure for Campus-based Laboratories at the University of Rijeka (RC.2.2.06-0001), which was co-funded from the European Fund for Regional Development.

LITERATURE CITED

Arita, M. and Jirka, G.H., 1987a. Two-layer model of saline wedge. I: Entrainment and interfacial friction. *Journal of Hydraulic Engineering*, 113(10), 1229–1246.

Arita, M. and Jirka, G.H., 1987b. Two-layer model of saline wedge. II: Prediction. *Journal of Hydraulic Engineering*, 113(10), 1249–1263.

Armi, L., 1986. The hydraulics of two flowing layers with different densities. *Journal of Fluid Mechanics*, 163, 27–58.

Balloffet, A. and Borah, D.K., 1985. Lower Mississippi salinity analysis. *Journal of Hydraulic Engineering*, 111(2), 300–315.

Baric, A.; Grbec, B., and Bogner, D., 2008. Potential implications of sea-level rise for Croatia. *Journal of Coastal Research*, 242(2), 299–305.

Bermudez, A. and Vázquez-Cendón, M.E., 1994. Upwind methods for hyperbolic conservation laws with source terms. *Computers & Fluids*, 23(8), 1049–1071.

Castro, M.J.; Ferreiro, A.M.; Garcia-Rodriguez, J.A.; Gonzales-Vida, J.M.; Macias, J.; Pares, C., and Vázquez-Cendón, E., 2005. The numerical treatment of wet/dry fronts in shallow flows: Application to one-layer and two-layer systems. *Mathematical and Computer Modelling*, 42(3–4), 419–439.

Castro, M.J.; Garcia-Rodriguez, J.A.; Gonzalez-Vida, J.M.; Macias, J., and Pares, C., 2007. Improved FVM for two-layer shallow-water models: Application to the Strait of Gibraltar. *Advances in Engineering Software*, 38(6), 386–398.

Castro, M.J.; Macias, J.; and Pares, C., 2001. A Q-scheme for a class of systems of coupled conservation laws with source term. Application to a two-layer 1D shallow water system. *ESAIM: Mathematical Modelling and Numerical Analysis*, 35(1), 107–127.

Castro, M.J.; Macias, J.; Peres, C.; Garcia-Rodriguez, J.A., and Vázquez-Cendón, E., 2004. Numerical simulation of two-layer shallow water flows through channels with irregular geometry. *Journal of Computational Physics*, 195(1), 202–235.

Cea, L.; Vázquez-Cendón, E.; Puertas, J., and Pena, L., 2004. Numerical treatment of turbulent and mass source terms in the shallow water equations for channels with irregular section. *In:* Neittaanmäki, P.; Rossi, T.; Korotov, S.; Oñate, E.; Périaux, J., and Knörzer, D. (eds.), *European Congress on Computational Methods in Applied Sciences and Engineering*. Jyvaskyla, Finland: ECCOMAS, pp. 1–17.

Dazzi, R. and Tomasino, M., 1974. Mathematical model of salinity intrusion in the delta of the Po River. *Coastal Engineering Proceedings*, 134, 2302–2321.

Dermissis, V. and Partheniades, E., 1985. Dominant shear stresses in arrested saline wedges. *Journal of Waterway, Port, Coastal, and Ocean Engineering*, 111(4), 733–752.

Farmer, D.M. and Armi, L., 1986. Maximal two-layer exchange over a sill and through the combination of a sill and contraction with barotropic flow. *Journal of Fluid Mechanics*, 164, 53–76.

Fofonoff, N. and Millard, R., 1983. Algorithms for Computation of Fundamental Properties of Seawater. *UNESCO Technical Papers in Marine Science*, 44, 53p.

Geyer, W.R. and Farmer, D.M., 1989. Tide-induced variation of the dynamics of a salt wedge estuary. *Journal of Physical Oceanography*, 19(8), 1060–1072.

Geyer, W.R. and MacCready, P., 2014. The estuarine circulation. *Annual Review of Fluid Mechanics*, 46, 175–197.

Geyer, W.R. and Ralston, D.K., 2011. 2.03—The dynamics of strongly stratified estuaries. *In:* Wolanski, E. and McLusky, D. (eds.), *Treatise on Estuarine and Coastal Science*. Amsterdam: Elsevier, pp. 37–52.

Geyer, W.R.; Scully, M.E., and Ralston, D.K., 2008. Quantifying vertical mixing in estuaries. *Environmental Fluid Mechanics,* 8(5), 495–509.

Grubert, J., 1989. Interfacial mixing in stratified channel flows. *Journal of Hydraulic Engineering*, 115(7), 887–905.

Hansen, D. and Rattray, Jr., M., 1966. New dimensions in estuary classification. *Limnology and Oceanography*, 11(3), 319–326.

Ibanez, C.; Pont, D., and Prat, N., 1997. Characterization of the Ebre and Rhone estuaries: A basis for defining and classifying salt-wedge estuaries. *Limnology and Oceanography*, 42(1), 89–101.

Intergovernmental Panel on Climate Change (IPCC), 2014. *Climate Change 2014: Synthesis Report: Summary Chapter for Policymakers*. Geneva, Switzerland: IPCC, 151p.

Karleuša, B.; Magaš, O.; Rubinić, J., and Palinić, N., 2009. Rječina River basin restoration (Croatia). *In:* Popovska, C. and Jovanovski, M. (eds.), *International Symposium on Water Management and Hydraulic Engineering*. Skopje, Macedonia: Ss. Cyril and Methodius University, pp. 873–884.

Karleuša, B.; Rubinić, J.; Radman, I.; Volf, G., and Krvavica, N., 2016. Cross-border water resources management in present conditions and for future scenarios. *In:* Karleuša, B. and Sušanj, I. (eds.), *Cross-Border Drinking Water Management*. Rijeka, Croatia: University of Rijeka, pp. 59–90.

Kay, D.J. and Jay, D.A., 2003. Interfacial mixing in a highly stratified estuary 1. Characteristics of mixing. *Journal of Geophysical Research*, 108(C3), 1–15.

Krvavica, N.; Mofardin, B.; Ružić, I., and Ožanić, N., 2012. Measurement and analysis of salinization at the Rječina estuary. *Gradevinar*, 64(11), 923–933.

Krvavica, N.; Travaš, V., and Ožanić, N., 2016. A field study of interfacial friction and entrainment in a microtidal salt-wedge estuary. *Environmental Fluid Mechanics*. In press.

La Rocca, M.; Adduce, C.; Lombardi, V.; Sciortino, G.; Hinkelmann, R., 2012a. Development of a lattice Boltzman method for two-layered shallow-water flow. *International Journal for Numerical Methods in Fluids*, 70(8), 1048–1072.

La Rocca, M.; Adduce, C.; Sciortino, G.; Bateman Pinzon, A., and Boniforti, M.A., 2012b. A two-layer, shallow-water model for 3D gravity currents. *Journal of Hydraulic Research*, 50(2), 208–217.

Liu, H.; Yoshikawa, N.; Miyazu, S., and Watanabe, K., 2015. Influence of saltwater wedges on irrigation water near a river estuary. *Paddy and Water Environment*, 13(2), 179–189.

Ljubenkov, I., 2015. Hydrodynamic modeling of stratified estuary: Case study of the Jadro River (Croatia). *Journal of Hydrology and Hydromechanics*, 63(1), 29–37.

MacDonald, D.G. and Geyer, W.R., 2004. Turbulent energy production and entrainment at a highly stratified estuarine front. *Journal of Geophysical Research C: Oceans*, 109(5), 1–17.

Mahgoub, M.; Hinkelmann, R., and La Rocca, M., 2015. Understanding the behaviour of gravity currents in tideless estuaries and considering the impact of sea level rise within the Nile Estuary. *Journal of Coastal Research*, 31(3), 714–722.

Monismith, S.G.; Kimmere, W.; Burau, J.R., and Stacey, M.T., 2002. Structure and flow-induced variability of the subtidal salinity field in northern San Francisco Bay. *Journal of Physical Oceanography*, 32(11), 3003–3019.

Murphy, A.H., 1988. Skill scores based on the mean square error and their relationships to the correlation coefficient. *Monthly Weather Review*, 116(12), 2417–2424.

Pawlak, G. and Armi, L., 1997. Hydraulics of two-layer arrested wedge flows. *Journal of Hydraulic Research*, 35(5), 603–618.

Pedersen, F.B., 1980. *A Monograph on Turbulent Entrainment and Friction in Two-Layer Stratified Flow*. Lyngby: Institute of Hydrodynamics and Hydraulic Engineering, Technical University of Denmark, 397p.

Peters, H., 1997. Observations of stratified turbulent mixing in an estuary: Neap-to-spring variations during high river flow. *Estuarine, Coastal, and Shelf Science*, 45(1), 69–88.

Ralston, D.K.; Geyer, W.R.; Lerczak, J.A., and Scully, M., 2010. Turbulent mixing in a strongly forced salt wedge estuary. *Journal of Geophysical Research: Oceans*, 115(C12), 1–19.

Rebollo, T.C.; Delgado, A.D., and Fernández-Nieto, E., 2003. A family of stable numerical solvers for the shallow water equations with source terms. *Computer Methods in Applied Mechanics and Engineering*, 192(1–2), 203–225.

Rezo, M. and Pavasović, M., 2014. Analiza mareografskih podataka o Jadranskome moru od 1953. do 2006. godine. *Geodetski list*, 4, 269–290 [in Croatian].

Rubinić, J. and Sarić, M., 2005. Hidrologija vodnih resursa u slivu Rječine. Water Resources Hydrology of the Rječina Catchment Area. *In:* Linić, A. (ed.), *Prošlost, Sadašnjost i Budućnost Vodoopskrbe i Odvodnje—Iskustva i Izazovi*. Opatija, Croatia, pp. 199–207 [in Croatian].

Sargent, F.E. and Jirka, G.H., 1987. Experiments on saline wedge. *Journal of Hydraulic Engineering*, 113(10), 1307–1323.

Schijf, J. and Schönfeld, J., 1953. Theoretical considerations on the motion of salt and fresh water. *Proceedings of the Minnesota International Hydraulics Convention* (Minneapolis, Minnesota), pp. 321–333.

Shaha, D.C.; Cho, Y.-K., and Kim, T.-W., 2013. Effects of river discharge and tide driven sea level variation on saltwater intrusion in Sumjin River Estuary: An application of finite-volume coastal ocean model. *Journal of Coastal Research*, 29(2), 460–470.

Sierra, J.P.; Sanchez-Arcilla, A.; Figueras, P.A.; Gonzales del Rio, J.; Rassmussen, E.K., and Mosso, C., 2004. Effects of discharge reductions on salt wedge dynamics of the Ebro River. *River Research and Applications*, 20(1), 61–77.

Stacey, M.T.; Rippeth, T.P., and Nash, J.D., 2011. 2.02—Turbulence and stratification in estuaries and coastal seas. *In:* Wolanski, E. and McLusky, D. (eds.), *Treatise on Estuarine and Coastal Science*. Amsterdam, Netherlands: Elsevier, pp. 9–36.

Stommel, H.M. and Farmer, H.G., 1952. *On the Nature of Estuarine Circulation: Part 1 (Chapters 3 and 4)*. Woods Hole Oceanographic Institution Technical Report, 131p.

Tsimplis, M.N.; Raicich, F.; Fenoglio-Marc, L.; Shaw, A.G.P.; Marcos, M.; Somot, S., and Bergamasco, A., 2012. Recent developments in understanding sea level rise at the Adriatic coasts. *Physics and Chemistry of the Earth*, *Parts A/B/C,* 40–41, 59–71.

Vázquez-Cendón, M.E., 1999. Improved treatment of source terms in upwind schemes for the shallow water equations in channels with irregular geometry. *Journal of Computational Physics*, 148(2), 497–526.

Xiao, H.; Huang, W.; Johnson, E.; Lou, S., and Wan, W., 2014. Effects of sea level rise on salinity intrusion in St. Marks River Estuary, Florida, U.S.A. *In:* Huang, W. and Hagen S.C. (eds.), *Climate Change Impacts on Surface Water Systems*. *Journal of Coastal Research*, Special Issue No. 68, pp. 89–96.

Yen, B., 2002. Open channel flow resistance. *Journal of Hydraulic Engineering*, 128(1), 20–39.

Yuan, R.; Zhu, J.R., and Wang, B., 2015. Impact of sea-level rise on saltwater intrusion in the Pearl River Estuary. *Journal of Coastal Research*, 31(2), 477–487.